ELSEVIER

CrossMark

Available online at www.sciencedirect.com

ScienceDirect

PHOTONICS AND NANOSTRUCTURES Fundamentals and Applications

Photonics and Nanostructures – Fundamentals and Applications 15 (2015) 53–58

www.elsevier.com/locate/photonics

Core–shell GaN–ZnO moth-eye nanostructure arrays grown on a-SiO_2/Si (1 1 1) as a basis for improved InGaN-based photovoltaics and LEDs

D.J. Rogers[a,*], V.E. Sandana[a], S. Gautier[b], T. Moudakir[b], M. Abid[b], A. Ougazzaden[b], F. Hosseini Teherani[a], P. Bove[a], M. Molinari[c], M. Troyon[c], M. Peres[d], Manuel J. Soares[d], A.J. Neves[d], T. Monteiro[d], D. McGrouther[e], J.N. Chapman[e], H.-J. Drouhin[f], R. McClintock[g], M. Razeghi[g]

[a] *Nanovation, 8 route de Chevreuse, Chateaufort 78117, France*
[b] *Georgia Institute of Technology/GT-Lorraine-UMI 2958 Georgia Tech-CNRS, 2-3 rue Marconi, Metz 57070, France*
[c] *LMEN, University of Reims Champagne-Ardennes, 21 rue Clement Ader, Reims 51685, France*
[d] *Departamento de Física/I3N, Universidade de Aveiro, Aveiro 3810-193, Portugal*
[e] *Department of Physics and Astronomy, University of Glasgow, Glasgow G12 8QQ, Scotland, UK*
[f] *Department of Irradiated Solids, Ecole Polytechnique, Palaiseau 91128, France*
[g] *Center for Quantum Devices, ECE Department, Northwestern University, Evanston, IL 60208, USA*

Received 11 June 2014; received in revised form 12 March 2015; accepted 22 March 2015
Available online 31 March 2015

Abstract

Self-forming, vertically-aligned, ZnO moth-eye-like nanoarrays were grown by catalyst-free pulsed laser deposition on a-SiO_2/Si (1 1 1) substrates. X-Ray Diffraction (XRD) and Cathodoluminescence (CL) studies indicated that nanostructures were highly *c*-axis oriented wurtzite ZnO with strong near band edge emission. The nanostructures were used as templates for the growth of non-polar GaN by metal organic vapor phase epitaxy. XRD, scanning electron microscopy, energy dispersive X-ray microanalysis and CL revealed ZnO encapsulated with GaN, without evidence of ZnO back-etching. XRD showed compressive epitaxial strain in the GaN, which is conducive to stabilization of the higher indium contents required for more efficient green light emitting diode (LED) and photovoltaic (PV) operation. Angular-dependent specular reflection measurements showed a relative reflectance of less than 1% over the wavelength range of 400–720 nm at all angles up to 60°. The superior black-body performance of this moth-eye-like structure would boost LED light extraction and PV anti-reflection performance compared with existing planar or nanowire LED and PV morphologies. The enhancement in core conductivity, provided by the ZnO, would also improve current distribution and increase the effective junction area compared with nanowire devices based solely on GaN.
© 2015 Elsevier B.V. All rights reserved.

Keywords: Nanostructures; InGaN; Photovoltaic; Anti-reflection; Moth-eye; ZnO

Since the emergence of p-type gallium nitride (GaN) in the early 1990s, there has been rapid industrial development for optoelectronic devices based on alloys of GaN with aluminum and indium ($Al_xGa_{1-x}N$ and

* Corresponding author.
E-mail address: rogers@nanovation.com (D.J. Rogers).

http://dx.doi.org/10.1016/j.photonics.2015.03.003
1569-4410/© 2015 Elsevier B.V. All rights reserved.

$In_xGa_{1-x}N$), which span a direct bandgap from the deep UV to the IR, and form the basis for commercial white (phosphor-assisted), UV and blue LEDs [1]. These alloy systems are now projected to also provide a platform for the development of novel multi-junction photovoltaics (PVs) having a direct tunable bandgap with an unparalleled fit to the solar spectrum combined with a relatively high carrier mobility and drift velocity. They also offer the capacity for operation under the demanding temperature and radiation requirements of concentration [2,3]. External quantum efficiencies reported up till now, however, have been rather disappointing [3,4]. This has been attributed to a number of factors, many of which can be addressed by nanostructuration. For instance, nanostructures generally offer higher materials quality than thin films on mismatched substrates, since relaxation and the high aspect ratio reduce the impact of interface issues with the substrate. The side-wall junctions in "core–shell" nanostructure architectures (see illustration below) are also an advantage in that they are inherently non-polar. This eliminates the detrimental band bending produced by the quantum-confined Stark effect encountered in conventional *c*-axis oriented planar GaN devices. Further potential benefits are increased junction area, lower defect density and less light trapping/reflection. Nanostructuration also brings significant new challenges, however, including issues with making good electrical contacts and with inhomogeneous electrical current flow through the, non-planar junction [5].

In previous work [6,7] it was shown that pulsed laser deposition (PLD) could be used to give self-forming arrays of vertically aligned nanostructures on a-SiO_2/Si and sapphire substrates. In particular, moth-eye-type nanostructures were shown to exhibit blackbody-like properties over the whole visible spectrum [8], which suggested that they could be used, for instance, as non-reflective coatings on solar cells [9] or for enhanced extraction in LEDs [10]. This paper reports on the use of such nanostructure arrays as templates for the growth of GaN by MOVPE.

ZnO moth-eye nanostructures were grown by PLD on a-SiO_2/Si (1 1 1) substrates, as described previously [11]. GaN was deposited on the ZnO nanostructures using a low pressure MOVPE T-shaped reactor [12] with trimethylgallium (TMG) as the Ga source and trimethylindium (TMIn) as the indium source. A combination of NH_3 and dimethylhydrazine (DMHY) was used as a source of atomic nitrogen. DMHY was added because of its' relatively low decomposition temperature, which enhanced the concentration of atomic nitrogen in the gas phase compared to NH_3 alone. This allowed GaN growth at lower initial growth temperatures than those used in conventional MOVPE deposition and thus avoided the back-etching of ZnO which occurs in NH_3 at temperatures over about 650 °C [13]. Nitrogen was employed as a carrier gas [14] during the whole growth process, instead of hydrogen, which can also promote back-etching of the ZnO surface at elevated temperatures [15]. Sample morphology was studied using a Hitachi S4800 Field Emission-Scanning Electron Microscope (FE-SEM). Cross-sectional samples were prepared and imaged in a dualbeam focused ion beam system (FEI Nova Nanolab 200). After electron beam deposition of a protective Pt layer ($\sim 6 \times 2\ \mu m^2$) on the GaN surface, the layer stack was milled through with a focused beam of Ga ions. The crystal quality of the nanostructures was investigated using high resolution X-ray diffraction (XRD) performed in a Panalytical MRD Pro system using Cu K_α radiation. Optical properties were studied using room temperature cathodoluminescence (CL) performed with a homemade system in an SEM [16]. RT specular reflection measurements were performed as a function of scattering angle and wavelength (in the range 450–720 nm) with an incidence angle fixed at 45°, as shown in Fig. 1.

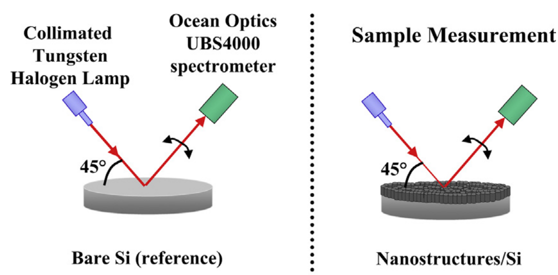

Fig. 1. Experimental set-up used for RT specular reflection measurements.

An Ocean Optics UBS4000 spectrometer and computer-controlled rotation stages were employed. The sample was illuminated with a collimated beam from a tungsten/halogen lamp. The rotation stages and the spectra acquisition were piloted with homemade software.

Fig. 2 shows SEM images of a ZnO/a-SiO_2/Si (1 1 1) sample before and after MOVPE growth of GaN.

In this figure, it can be seen that the nanocones thicken and become more rounded after the GaN growth, which is coherent with GaN having encapsulated the ZnO. The GaN also appears to have a mottled surface compared to the ZnO.

Fig. 3 shows a FE-SEM image of the FIB-milled cross-section.

The sample shows distinct, continuous GaN and ZnO layers with a smooth interface. The surface mottling of

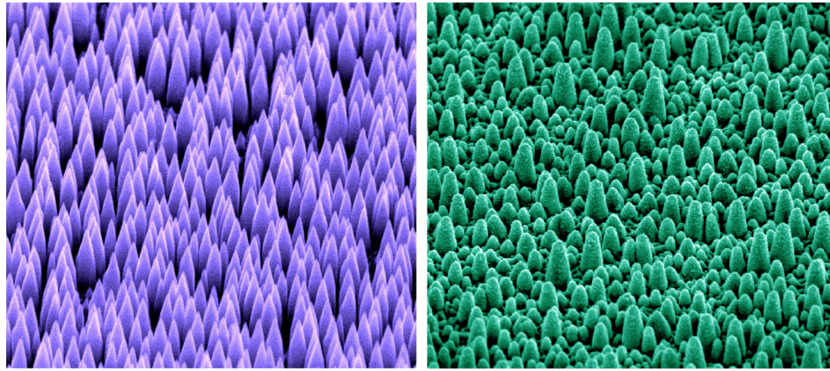

Fig. 2. FE-SEM images of a nano $ZnO/a-SiO_2/Si$ (1 1 1) sample before and after MOVPE overgrowth of GaN.

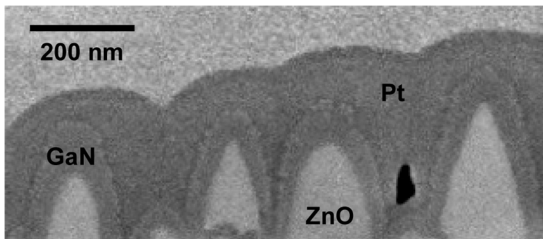

Fig. 3. An FE-SEM image of an ion-milled cross-section of the $GaN/ZnO/a-SiO_2/Si$ (1 1 1). The chemical identity of each layer was confirmed by Energy Dispersive X-ray (EDX) analysis.

the GaN that was apparent in Fig. 2 can also be seen. The thickness of the GaN layer was estimated to be about 130 nm.

XRD $2\theta/\omega$ scans revealed (0 0 0 2) oriented wurtzite structure for the ZnO and GaN/ZnO. Fig. 4 shows normalized $2\theta/\omega$ scans for the (0 0 0 2) peak before and after MOVPE growth of GaN.

A strong (0 0 0 2) reflection is observed before and after GaN growth, which suggests that the preferential c-axis orientation was maintained. The nano ZnO peak shows broadening on the higher-angle side, signifying a region with a smaller c-lattice parameter. It has been suggested that this could be due to disorder at the start of growth creating a less dense a–b plane at the base of the nanocones (and thus a larger a lattice parameter) [17]. The peak broadens after the GaN growth (FWHM of 0.061° vs a value of 0.019° before GaN growth), which is what might be expected for epitaxy of a thin layer of GaN. The main peak position in the $2\theta/\omega$ scans after GaN growth has a c-lattice parameter of 5.204 Å, as compared to the value of 5.203 Å for the ZnO prior to GaN growth. This is very close to the equilibrium value expected for wurtzite ZnO (5.206 Å) and significantly higher than the equilibrium value of 5.186 Å, for wurtzite GaN which we observe typically for planar GaN layers grown on ZnO thin film templates [13]. A similar shift in the GaN peak position has, however, been observed for certain growth conditions of planar GaN layers on ZnO thin film templates and attributed to compressive epitaxial strain in the GaN layer [18]. This is, in fact, a potential advantage compared to the unstrained n-GaN core on which the InGaN absorber is grown in conventional GaN core–shell structures (see Fig. 5) in that the lattice parameter offers a better match to InGaN with the higher indium contents required for both the quantum wells of green LEDs and the absorber layer of solar cells.

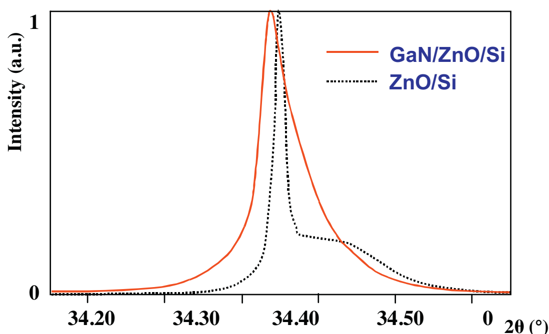

Fig. 4. Normalised XRD $2\theta/\omega$ scans around the (0 0 0 2) peak of the nanostructured ZnO on $a-SiO_2/Si$ (1 1 1) before and after MOVPE GaN overgrowth.

XRD ω rocking curves around the (0 0 0 2) peak revealed a FWHM that increased from 0.85° to 1.07° after GaN growth. In a recent study of ZnO nanostructure arrays, the authors reported that the absolute values of the ω rocking curve corresponded closely to the dispersion in the physical orientation of the nanostructures about the normal to the substrate surface [19].

Fig. 6 shows the RT CL spectra for the sample luminescence before and after GaN growth.

Both spectra exhibit an ultraviolet (UV) band (at around 380–382 nm), which is characteristic of Near

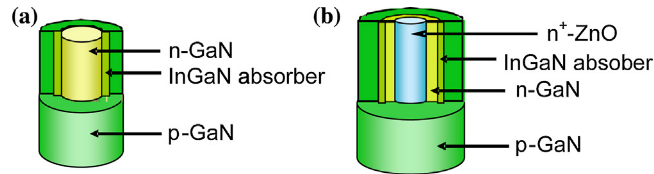

Fig. 5. Illustrations of (a) a conventional core–shell InGaN-based nanowire p–n junction (b) the novel InGaN-based p–n junction architecture with a ZnO core.

Band Edge (NBE) emission from wurtzite ZnO [20]. The CL spectrum for the ZnO nanocones has a high intensity ratio between the NBE and green deep level emission band, which indicates that the nanostructures had particularly good crystal quality. After GaN growth, a pronounced yellow/green band appeared (peaked at about 540 nm). A comparable band was observed in previous studies of GaN films grown on 2D ZnO buffer layers and it was suggested that it could be associated with defects in the wurtzite GaN structure [21]. Similar, yellow/green emission has also been linked to surface related defects in GaN nanostructures.

Fig. 7 shows the results of reflection measurements for (a) the a-SiO_2/Si (1 1 1) substrate and (b) the moth-eye GaN/ZnO/a-SiO_2/Si (1 1 1), with intensity expressed relative to the maximum reflectance for the Si (1 1 1) substrate. The plots show that the reflectance from the moth-eye nanostructures is less than 1% of that for a bare substrate over the whole visible wavelength range of 400–720 nm and at all scattering angles up to 60°. Fig. 7 also reveals a diffuse signal of ∼0.4% for the nanostructured surface, which is suppressed for wavelengths under ∼550 nm. This transition corresponds to the luminescence cut-off observed in the CL studies and is coherent, therefore, with a diffuse signal originating from PL of the GaN rather than light scattering. The general absence of significant diffuse scattering in the sub-500 nm range (<0.4% total reflection) is also coherent with the sub-visible scale of the nanostructures acting as a graded effective refractive index at the air interface, as suggested in previous studies on the reflectance of ZnO moth-eye nanostructure arrays. This excellent anti-reflection performance appears to be enhanced by the tapering form, the strong alignment and the randomized nanocone heights, which all act to smooth the transition in refractive index and eliminate diffuse scattering.

Adoption of such a ZnO core in the nanostructure also offers a potential solution to inhomogeneous current flow issues because, unlike GaN, ZnO can be degenerately doped and highly conductive (indeed, it is currently displacing indium tin oxide as a transparent electrode in many industrial applications [22]). Such an enhancement in core conductivity would significantly improve current distribution and increase the effective junction area, as illustrated in Fig. 8.

In conclusion, self-forming, vertically-aligned, arrays of moth-eye-like ZnO nanocones grown by PLD were adopted as templates for the overgrowth of non-polar GaN by MOVPE. XRD, SEM, EDX and CL revealed that the ZnO was encapsulated with GaN, without evidence of ZnO back-etching. A shift in XRD (0 0 0 2) peak for GaN was attributed to compressive epitaxial strain in the GaN. This provides a better lattice parameter match to InGaN with higher indium contents and can thus act

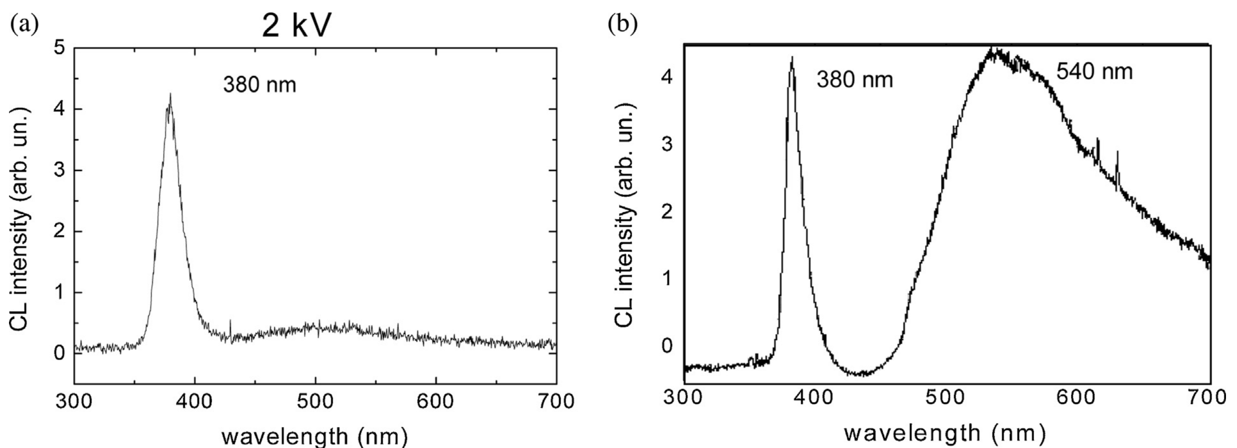

Fig. 6. CL spectra for a sample of moth-eye ZnO/a-SiO_2/Si (1 1 1) (a) before and (b) after growth of GaN by MOVPE.

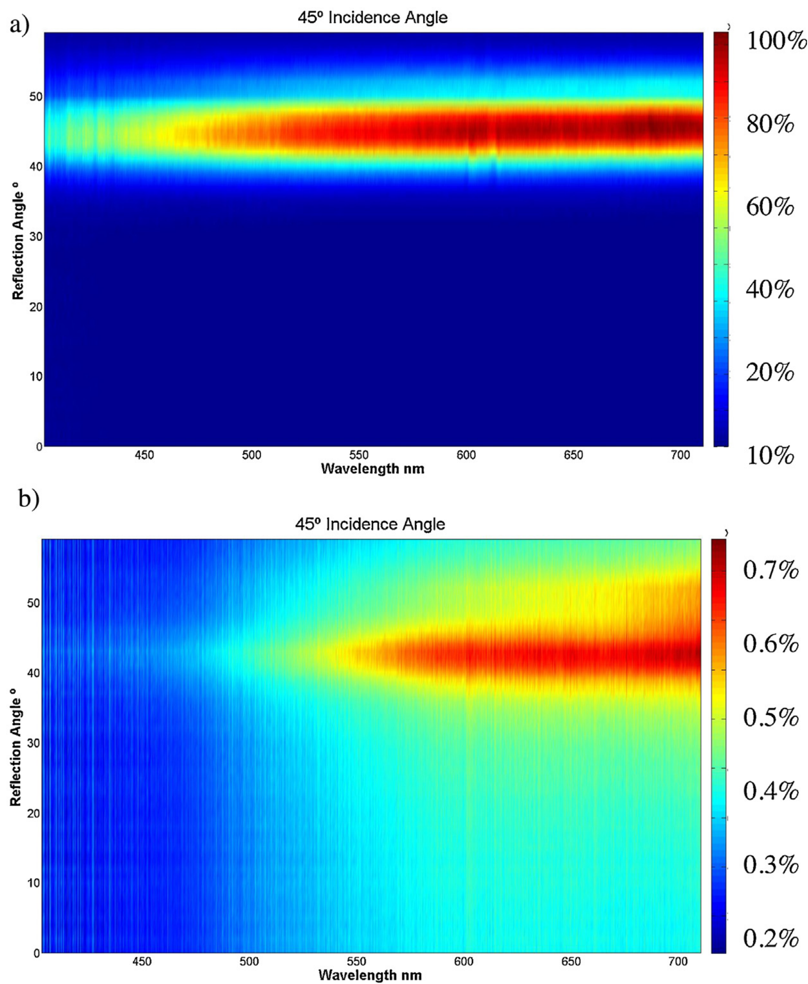

Fig. 7. Optical reflectance as a function of scattering angle and wavelength for (a) the a-SiO_2/Si (1 1 1) substrate and (b) the moth-eye GaN/ZnO/a-SiO_2/Si (1 1 1) (with the incident beam held at a fixed incidence angle of 45 degrees from the normal to the sample surface).

to promote enhanced absorption in solar cells [22] or combat the LED "green gap" [23].

Since ZnO nanostructures can be grown more readily than GaN on nearly all substrates [24], such an approach could also facilitate growth of GaN based nanostructures, thin films and devices on mismatched and/or technologically important substrates, which may have been inaccessible till present.

Angular-dependent specular reflection measurements indicated that the GaN/ZnO nanostructures were remarkably black-body-like with less than 1% of the reflectance for a bare substrate over the whole visible wavelength range of 400–720 nm and at all scattering angles up to 60°. Such characteristics would boost LED light extraction and PV anti-reflection performance compared with existing planar and nanowire morphologies.

Finally, the adoption of a transparent and conductive GaN-shell/ZnO-core configuration offers the perspective of more efficient nanostructured devices due to a more homogeneous current distribution and an increased effective junction area.

Overall, improved PV and LED performance can be expected (particularly in the green part of the spectrum) compared with existing GaN-based device architectures.

Acknowledgements

The authors would like to thank the French "Agence Nationale de la Recherche" for financial support and the Centre Technologique Universitaire at the "Institut d'Electronique Fondamentale" of Orsay University for access to the XRD facilities. Acknowledgements to FCT

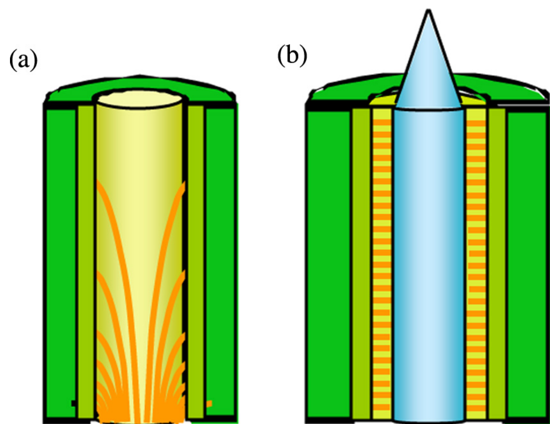

Fig. 8. Illustrations of (a) inhomogeneous current flow (in orange) for the n-type GaN layer in a conventional core–shell InGaN-based nanowire p–n junction (b) improved current distribution and increased effective junction area in the novel GaN-based p–n junction architecture with highly conductive ZnO (in blue) acting as an equipotential core. (For interpretation of the references to color in this figure legend, the reader is referred to the web version of this article.)

for the funding of RECI/FIS-NAN/0183/2012 (FCOMP-01-0124-FEDER-027494) project is also due.

References

[1] S.P. DenBaars, D. Feezell, K. Kelchner, S. Pimputkar, C.-C. Pan, C.-C. Yen, S. Tanaka, Y. Zhao, N. Pfaff, R. Farrell, M. Iza, S. Keller, U. Mishra, J.S. Speck, S. Nakamura, Acta Mater. 61 (2013) 945.
[2] L. Hsu, W. Walukiewicz, J. Appl. Phys. 104 (2008) 24507.
[3] C.A.M. Fabien, M. Moseley, B. Gunning, W.A. Doolittle, A.M. Fischer, Y.O. Wei, F.A. Ponce, IEEE J. Photovoltaics 4 (2014) 2.
[4] A.G. Bhuiyan, K. Sugita, A. Hashimoto, A. Yamamoto, IEEE J. Photovoltaics 2 (2012) 276.
[5] B.J. Connors, Simulation of Current Crowding Mitigation in GaN Core–Shell Nanowire LED Designs, Georgia Institute of Technology, 2011 (PhD Thesis).
[6] V.E. Sandana, D.J. Rogers, F.H. Teherani, R. McClintock, M. Razeghi, H.-J. Drouhin, M.C. Clochard, V. Sallet, G. Garry, F. Fayoud, Proc. SPIE 6895 (2008) 68950Z.
[7] V.E. Sandana, D.J. Rogers, F.H. Teherani, R. McClintock, C. Bayram, M. Razeghi, H.-J. Drouhin, M.C. Clochard, V. Sallet, G. Garry, F. Falyouni, J. Vac. Sci. Technol. B 27 (3) (2009) 1678–1683.
[8] M. Peres, M.J. Soares, A.J. Neves, T. Monteiro, V.E. Sandana, F. Teherani, D.J. Rogers, Phys. Stat. Sol., B 247 (2010) 1695–1698.
[9] L. Tsakalakos, Mater. Sci. Eng. Res. 62 (2008) 175–189.
[10] J. Zhong, H. Chen, G. Saraf, Y. Lu, C.K. Choi, J.J. Song, Appl. Phys. Lett. 90 (2007) 203515.
[11] D.J. Rogers, V.E. Sandana, F. Hosseini Teherani, M. Razeghi, H.-J. Drouhin, Proc. SPIE 7217 (2009) 721708.
[12] A. Mircea, A. Ougazzaden, R. Mellet, Prog. Cryst. Growth Charac. 19 (1989) 39.
[13] D.J. Rogers, F. Teherani, A. Ougazzaden, S. Gautier, L. Divay, A. Lusson, O. Durand, F. Wyczisk, G. Garry, T. Monteiro, M. Correira, M. Peres, A. Neves, D. McGrouther, J. Chapman, M. Razeghi, Appl. Phys. Lett. 91 (2007) 071120.
[14] S. Gautier, J. Ould-Saad, A. Martin, A. Sirenko, A. Ougazzaden, J. Cryst. Growth 298 (2007) 428.
[15] F. Scholz, V. Harle, F. Steuber, H. Bolay, A. Dornen, B. Kaufmann, V. Syganow, A. Hangleiter, J. Cryst. Growth 170 (1997) 321.
[16] M. Troyon, D. Pastré, J.P. Jouart, J.L. Beaudoin, Ultramicroscopy 75 (1998) 15.
[17] V.E. Sandana, D.J. Rogers, F. Hosseini Teherani, P. Bove, M. l Molinari, M. Troyon, A. Largeteau, G. Demazeau, C. Scott, G. Orsal, H.-J. Drouhin, A. Ougazzaden, M. Razeghi, Phys. Status Solidi C 10 (10) (2013) 1317.
[18] D.J. Rogers, A. Ougazzaden, V.E. Sandana, T. Moudakir, A. Ahaitouf, F. Hosseini Teherani, S. Gautier, L. Goubert, I.A. Davidson, K.A. Prior, R.P. McClintock, P. Bove, H.-J. Drouhin, M. Razeghi, Proc. SPIE 8263 (2012) 82630R–82631R.
[19] R. Erdelyi, T. Nagata, D.J. Rogers, F.H. Teherani, Z. Horvath, Z. Labadi, Z. Baji, Y. Wakayama, J. Volk, Cryst., Growth Des. 11 (2011) 2515–2519.
[20] Y.C. Kong, D.P. Yu, B. Zhang, W. Fang, S.Q. Feng, Appl. Phys. Lett. 78 (2001) 407.
[21] A. Ougazzaden, D.J. Rogers, F. Hosseini Teherani, G. Orsal, T. Moudakir, S. Gautier, V.E. Sandana, F. Jomard, M. Abid, M. Molinari, M. Troyon, P.L. Voss, D. McGrouther, J.N. Chapman, Proc. SPIE 7603 (2010) 76031D–76041D.
[22] D.J. Rogers, F. Hosseini Teherani, Encyclopedia of Materials Science & Technology, Elsevier, Oxford, 2010, pp. 1–5.
[23] D.J. Rogers, F. Hosseini Teherani, P. Bove, R. McClintock, M. Razeghi, SPIE Newsroom (2012), http://dx.doi.org/10.1117/2.1201206.004238.
[24] D.J. Rogers, F. Hosseini Teherani, V.E. Sandana, M. Razeghi, Proc. SPIE 7605 (2010), 7676050K-1–76050K-11.